A simple model for breakup time prediction of Water-Heavy Fuel Oil emulsion droplets

Stavros Fostiropoulos[*1,2], George Strotos[3], Nikolaos Nikolopoulos[1] and Manolis Gavaises[2]

[1]Centre for Research and Technology Hellas/Chemical Process and Energy Resources Institute (CERTH/CPERI), Egialeias 52, Marousi, Greece

[2]City University of London, School of Engineering and Mathematical Sciences, Northampton Square, EC1biliV 0HB London, UK

[3]University of Thessaly, 41110 Larissa, Greece

[*]Corresponding author: M.Gavaises@city.ac.uk

Abstract

Immiscible heavy fuel-water (W/HFO) emulsion droplets inside combustion chambers are subjected to explosive boiling and fragmentation due to the different boiling point between the water and the surrounding host fuel. These processes, termed as either puffing or micro-explosion, are investigated with the aid of a CFD model that solves the Navier-Stokes and energy conservation equations alongside with three sets of VoF transport equations resolving the formed interfaces. The model is applied in 2-D axisymmetric configuration and it is valid up to the time instant of HFO droplet initiation of disintegration, referred to as breakup time. Model predictions are obtained for a wide range of pressure, temperature, water droplet surface depth and Weber number; these are then used to calibrate the parameters of a fitting model estimating the initiation breakup time of the W/HFO droplet emulsion with a single embedded water droplet. The model assumes that the breakup time can be split in two distinct temporal stages. The first one is defined by the time needed for the embedded water droplet to heat up and reach a predefined superheat temperature and a vapor bubble to form; while the succeeding stage accounts for the time period of vapor bubble growth, leading eventually to emulsion droplet break up. It is found that the fitting parameters are ±10% accurate in the examined range of We <220, T <2000 K, P <140 bar and $\delta < 0.15$.

Keywords: Fuel-water emulsion, breakup, heat convection, explosive boiling

Nomenclature

Roman symbols

a	Thermal diffusivity [m^2s^{-1}]
b	Scriven bubble growth factor
c_p	isobaric heat capacity [J kg^{-1} K^{-1}]
d	Distance [m]
D	Diameter [m]
E	Energy [J]
g	Correction function
h_{lv}	heat of vaporization [J kg^{-1}]
Ja	Jakob number ($\rho_w c_{p,w} \Delta T_s / \rho_v h_{lv}$) [-]
k	thermal conductivity [W m^{-1} K^{-1}]
m	mass [kg]
Oh	Ohnesorge number ($\mu_f / \sqrt{\rho_f \sigma D_f}$)[-]
p	pressure [Pa]
Pe_f	Peclet number ($D_f u_f / a$) [-]
R	radius [m]
Re	Reynolds number ($\rho_g u_g D_f / \mu_g$) [-]
St	Stefan number ($c_{p,w} \Delta T_s / h_{lv}$) [-]
t	Time
T	temperature [K]
u	Velocity [ms^{-1}]
V	Volume [m^3]
We	Weber number ($\rho_g u_g^2 D_f / \sigma$) [-]

Greek symbols

β	Growth factor
δ	Surface depth (m)
ΔT_s	Superheat degree [K]
μ	Dynamic viscosity [Pa s]
ρ	density [kg m^{-3}]
σ_{gf}	Surface tension (gas-fuel) [N m^{-1}]

Subscripts

∞	far-field quantity
0	initial value
b	bubble
br	breakup
CFD	values provided by CFD
f	fuel phase/droplet
g	gas
i	interface
sat	saturated
v	Vapor
w	water

1. Introduction

Despite the global efforts for electrification of the transport sector, heavy-duty and marine Diesel engines are extensively used as a source of power, since they provide high power output, the highest thermodynamic and well-to-wheel efficiencies as well as low fuel cost. Over the next two decades it is expected that the usage of liquid fossil fuel will increase by 25% globally, while the demand of liquid fuels just for heavy-duty vehicles is forecasted to increase by more than 50% [1]. Still, despite their advantages, Diesel engines are one of the major atmospheric pollutant contributors, such as NOx and particulate matter (PM). The aforementioned concerns have motivated policy makers and engine manufacturers to introduce more rigid and strict emission regulations [2, 3]; among them, water-emulsified fuels can simultaneously reduce both NOx and PM emissions [4] without increasing cost.

In W/HFO emulsions water is dispersed in the form of fine immiscible droplets inside the parent fuel droplet. The emulsified fuel is prepared with mechanical agitation and the presence of surfactant agents in order to avoid coalescence of the water sub-droplets. When the emulsified fuel is sprayed inside the hot combustion chamber, heat is initially transferred at the surface of the parent fuel droplets. Since the fuel component has higher boiling point compared to that of water sub-droplets, the latter becomes superheated and starts to boil [5], creating vapor expansion; that, in turn, leads to fragmentation of the parent oil droplet that eventually breaks up [6-8] and thus, improving gas-fuel mixing due to faster vaporisation. Two processes, termed as micro-explosion and puffing, may prevail: puffing is defined as the process during which partial breakup of the parent fuel droplet occurs [9], while micro-explosion is the complete breakup of the fuel droplet into small droplets [10].

Puffing and micro-explosion processes have been mainly investigated through experimental campaigns. However, most of them have focused on the combustion characteristics and pollutant formation at the macroscopic level of engine performance; see indicatively [11-13]. Regarding single droplet emulsion experiments, the mechanism of homogeneous explosive boiling was first studied by [14] where the size of a growing vapor bubble, inside a superheated water droplet was measured. Significant factors that may affect the emulsion breakup outcome were found to be the water volume fraction [15], the quantity of surfactant [16] and the size distribution [17] of the water sub-droplets. In the works of [18, 19] the breakup outcome of a water-fuel droplet subjected to conductive, convective and radiation heating was investigated. In the recent work of [20] characterization of breakup of an emulsion droplet was reported while the characterization of size, temperature and location of embedded water droplets was investigated by [21] during micro explosions. Finally, in the work of [22], a phenomenological description of the vaporization process during emulsion droplet heating is reported. The aforementioned experiments have been performed with relatively larger droplets (O (1 mm)) compared to those realized in engines.

Recently, single droplet experiments having sizes similar to those realised in fuel sprays (O (10 μm)), were performed by [23, 24]. Puffing was observed more often than micro-explosion, resulting to fine droplets. Still, besides the important conclusions drawn, the breakup mechanism was difficult to visualize due to the short timescale O (10 μs) and the small fuel droplet size.

Development of micro-explosion models has recently been attempted; a number of simplified mathematical models have been suggested [25-28] and they are of interest to the present work. In the work of [27] a mathematical model is presented describing the growth of a vapor bubble inside a water droplet placed inside a liquid pool. Besides the simplifications considered, the results of the model were found to be in good agreement against the experiment of [29]. A similar configuration was employed in the breakup model of [28] that performed a stability analysis for predicting the droplet size and velocity. A more complex configuration was investigated in [26]; the embedded water droplet was located at the centre of a fuel droplet and the time period needed for the former to reach its boiling degree was predicted. Although this model ignores water-vapor bubble formation and growth, the predicted puffing time was in reasonable agreement with the relevant experimental results. More sophisticated CFD models can in principle provide further insight into the physical mechanisms of micro-explosion of emulsions but so far, only few relevant studies have been reported due to the enormous computation time required. Along these lines, the numerical simulations of [30] have shed light on the complex evolution of puffing and micro-explosion phenomena for a predefined location and size of the water-vapor bubble. The heating process of emulsion droplets has been studied by [31], concluding that the flow inside the droplet and the fuel Peclet number define the time needed for the water droplets to become superheated and start boiling. Recently, in the CFD work [32] from the authors, the droplet heating up to water-vapor expansion and droplet fragmentation were simulated and the corresponding time needed for those processes to occur was predicted. The latter was observed to be faster compared to the aerodynamic-induced breakup of a neat HFO droplet exposed to the same surrounding gas flow conditions, suggesting that fuel emulsification is beneficial for viscous fuels, such as HFO. In the present work, this model is further applied to a wide range of conditions for which no prior experiments or simulations exist; namely We and $p-T$ values ($40 < We < 200,\ 10 < p < 140$ bar, $600 < T < 2000$ K) including also those typically realised in marine engines during the main injection phase ($p \sim 120$ bar, $T \sim 900$ K). The emulsion droplet diameter and gas stream velocity range, correspond to the aforementioned We range, are 50 μm and $40 < u_g < 100$ m/s, respectively. From the numerical simulations, two distinct timescales are estimated: the heating time until the water boiling initiation and the vapor bubble growth time until fuel droplet break up. These results are subsequently used to derive a fitting model predicting the W/HFO emulsion breakup initiation time. The numerical methods used, scope and rational for suggesting the

proposed correlations for this wide range of conditions, that has been documented in a number of relevant previous works of the authors [33-37] is to overcome the restrictions imposed by the enormous computational time required by CFD simulations while they further resolve the limitation of mesh resolution realized when small water droplet sizes (1 μm) are located at the proximity of the HFO-gas interface. In the works of [33, 36, 37] the aerodynamic induced breakup of a single droplet and droplets in tandem was investigated while in [34, 35] heat transfer and evaporation of a single fuel droplet was simulated. The derived fitting model is suitable for implementation to widely used fuel spray simulation codes utilizing the Eulerian-Lagrangian approach [38] for resolving the development of sprays consisting of multi-million droplets. In the following sections, the mathematical description of the derived model is presented, alongside with the discussion of the obtained results and the most important conclusions.

2. Model description

2.1 CFD model-Examined cases

As already mentioned, the CFD model of [32] is employed to examine a configuration where a single spherical water sub-droplet ($D_w = 10$ μm) is located inside a fuel droplet ($D_f = 50$ μm) as shown in Figure 1 (left panel); note that the figure is not in scale. Equations are solved in an axisymmetric domain where the left vertical axis is a velocity inlet boundary that imposes the velocity of the stream flow, while the rest boundaries are open and the velocity gradient is set to zero. Three VoF equations are employed to resolve the water-fuel, fuel-gas and water-vapor-fuel interfaces, respectively. Each VoF equation is spatially discretised using the compressive scheme [39], while the momentum equations are spatially discretized with a second order upwind scheme; a first order upwind scheme is employed for the spatial discretisation of the energy conservation equation. Moreover, an adaptive local refinement technique is employed [40], as it further enhances the resolution of the computations at the interface regions. Starting from a course base grid resolution of 2cpR, a resolution of 200cpR is finally achieved with 6 levels of refinement

The emulsion droplet is initially placed at ambient gas with pressure p and temperature T_∞ (range of values is illustrated in Table 1), while the initial fuel temperature is T_0 (360 K). Evaporation of the parent fuel droplet is ignored, since its timescale is much longer compared to that of emulsion breakup [30]. The examined properties are similar to that of a highly viscous HFO, while the preheating temperature of the fuel and the ambient conditions examined ($p = 90$ bar, $T = 900$ K) are typically met in large marine Diesel engines. Since a 2-D axisymmetric domain is adopted, the embedded water droplet can only be located

on the axis of symmetry. Fuel density, dynamic viscosity and surface tension can be found in the work of [41], while thermal conductivity and heat capacity are computed by empirical relationships provided in [42]; these properties were assumed constant at (p, T_0) without accounting for their slight change due to droplet heating, while the surrounding gas properties were computed at (p, T_∞). Model predictions have been obtained as function of the water droplet location inside the parent droplet, We and $p-T$ conditions, summarized in Table 1; in all simulations performed, one parameter is changed each time. For the cases 1 to 4, where the gas temperature is varied, the corresponding change in the gas properties is compensated by a corresponding change in the gas stream velocity in order to keep the We number constant. In cases 5 to 7, the effect of the dimensionless distance δ of the water sub-droplet from the from the HFO-gas interface ($\delta = d_h/R_f$) is examined; δ approaching 0 indicates that the water droplet approaches this interface. The effect of water content is not examined here. In practice, a wide range of water droplet sizes will appear in emulsion droplets; such cases require a 3-D approximation which is impossible to resolve since enormous CPU resources are required. Finally, it is pointed out that the effect of Nusselt, Peclet, Prandtl, Biot and Stanton numbers, which are relevant in heat transport processes, has also not been examined. This is justified as the variation of the HFO physical properties in the examined range of temperatures is not significant, while at the same time, the study of lighter fuels is out of scope in the present work, as water emulsions are not utilised in practice. On the contrary, the variation of the We number is relevant since it controls the aerodynamic-induced deformation of the parent droplet.

	T_∞	p	We	d_h/R_f		T_∞	p	We	d_h/R_f
ref	1000	30	68	0.06	**Case 8**	1000	30	40	0.06
Case 1	700	30	68	0.06	**Case 9**	1000	30	92	0.06
Case 2	800	30	68	0.06	**Case 10**	1000	30	136	0.06
Case 3	1200	30	68	0.06	**Case 11**	1000	30	188	0.06
Case 4	1400	30	68	0.06	**Case 12**	1000	10	68	0.06
Case 5	1000	30	68	0.02	**Case 13**	1000	50	68	0.06
Case 6	1000	30	68	0.05	**Case 14**	1000	100	68	0.06
Case 7	1000	30	68	0.15	**Case 15**	1000	120	68	0.06

Table 1. Operating conditions for the examined cases. For all cases Oh~0.9

Demonstration of the temporal evolution of emulsion droplet heating and fragmentation for an indicative case is illustrated in the right panel of Figure 1; At $t = 3$ μs, the appearance of a water-vapor bubble is

observed at the proximity of the HFO-water interface after the criteria for the water-vapor generation have been fulfilled [32]. Then the bubble grows and at some time instant ($t = 4.7$ μs) it reaches the HFO-gas interface, allowing it to escape into the surrounding ambient gas.

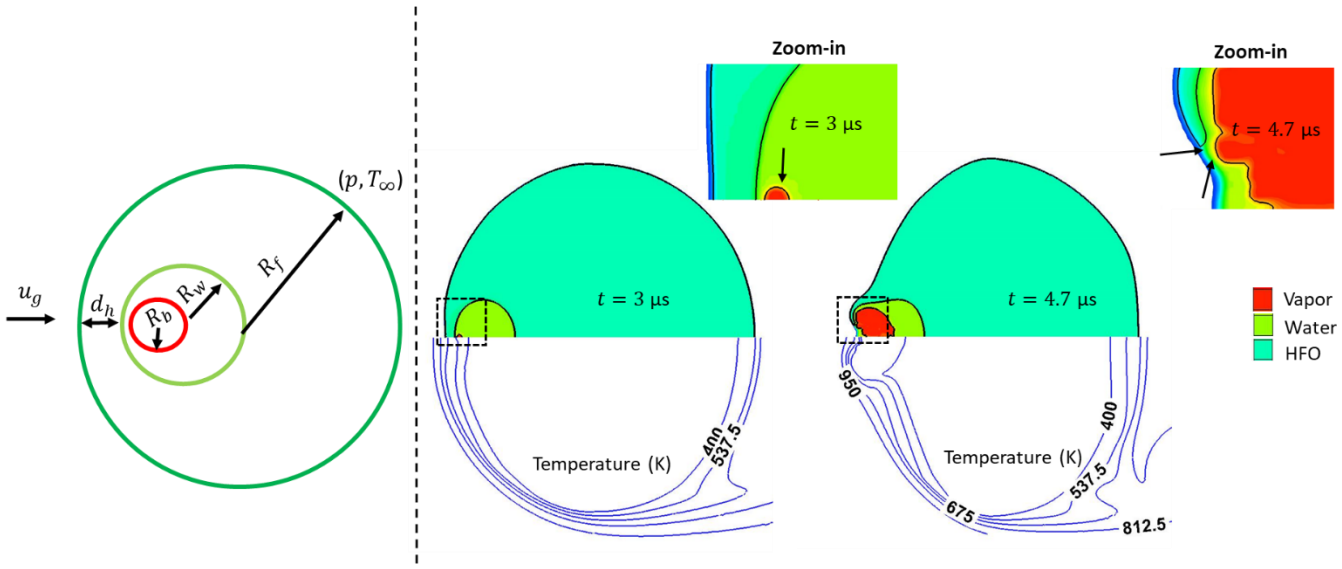

Figure 1. Model configuration (left panel) and temporal evolution of emulsion droplet breakup (right panel) where HFO, water and vapor phases are indicated by blue, green and red colours, respectively

2.2 Break-up initiation time fitting model

The correlations of this model are based on the assumption that the emulsion-induced breakup time can be split into two distinct time periods (Eq. 1): (i) the time period t_h of water droplet heating from its initial temperature T_0 up to a superheated one $T'_{sat} = T_{sat} + \Delta T_s$ where the formation of a tiny water-vapor bubble is realized; (ii) the subsequent time period t_{grow} during which the water-vapor bubble grows up until the HFO-gas interface eventually breaks up.

$$t_{br} = t_h + t_{grow} \tag{1}$$

The time period t_h depends mostly on a heat convection time t_{conv} inside the fuel phase, as shown in Eq. 2. This assumption is valid since the fuel Peclet number ($Pe_f = D_f u_f / a$) is in the range 3000-7000. The characteristic velocity magnitude u_f is computed as reported in [43, 44] and it is based on the gas-fuel density ratio and the gas stream velocity. While t_{conv} forms the basis for the estimation of t_h, three empirical coefficients (f_{We}, f_T and f_δ) have been considered to quantify the influence of We $(0 - 200)$, gas temperature $(600 < T_\infty < 2000)$ and location δ $(0 - 0.15)$ of the water droplet from the HFO-gas interface. The derivation of these coefficients, shown in Appendix 1, is based on the superposition principle without accounting for any interdependencies between the parameters examined; the validity of this assumption is discussed in sub-section 3.4.

$$t_h = C \cdot t_{conv} \cdot f_T \cdot f_\delta \cdot f_{We}, \quad C = 3.6$$

$$u_f = u_g \sqrt{\frac{\rho_g}{\rho_f}}$$

$$f_T = \left(\frac{T'_{sat} - T_0}{T_\infty - T_0} \right)^{0.4} \tag{2}$$

$$f_\delta = 1 + 8.9 \cdot \delta$$

$$f_{We} = We^{-0.22}$$

It can be observed that the heating time decreases with increasing gas temperatures and We. Moreover, a preheated water droplet at the saturation temperature will have zero heating time (i.e. vapor will form instantly); on the contrary, for a water sub-droplet approaching the HFO-gas interface ($\delta = 0$), the bubble will not form instantly and a finite time is needed to reach the required superheated temperature.

Turning now to t_{grow}, the Scriven's solution [45] initially serves as the basis for its derivation (see Appendix B for further details); the values of the coefficients g_{br}, g_p, g_T and g_{We}, accounting for the influence of pressure ($10 < p < 140$ bar), gas temperature ($600 < T_\infty < 2000$) and We $(0 - 200)$, have been determined after calibration with the corresponding CFD results. Note here that for small We and $p - T$ values, the corresponding coefficients tend to unity ($g_p g_T g_{We} = 1$), indicating that Scriven's theory is valid for those conditions without imposing any modifications. The relationship for t_{grow} alongside with that for the implemented correction factors reads:

$$t_{grow} = \left(\frac{R_w^2}{a_w} \frac{1}{\beta^2} \right) \cdot \left(\frac{g_{br}}{g_p g_T g_{We}} \right)^2$$

$$\beta = \sqrt{\frac{12}{\pi}} \left\{ \frac{\Delta T_s}{\left(\frac{\rho_g}{\rho_w} \right) \left[\frac{h_{lv}}{c_{p,w}} + \left(\frac{c_{p,w} - c_{p,g}}{c_{p,w}} \right) \Delta T_s \right]} \right\}$$

$$g_{br} = 0.5 + 30 \cdot We^{-1.5} \tag{3}$$

$$g_p = 1 + 0.36 \cdot \left(\frac{p}{p_{ref}} \right)^{2.21}$$

$$g_T = 1 + 0.28 \cdot \left(\frac{T_\infty - T_0}{T_{\infty,ref}} \right)^{-0.7}$$

$$g_{We} = 1 + 0.008 \cdot We^{0.9}$$

3. Discussion

3.1 Overall performance

Predictions for the breakup time obtained from the above correlations are shown in Figure 2 along with those predicted from the CFD simulations for the conditions of Table 1. The 45° line is also illustrated (black solid line); ideally all CFD simulation points should lie on this line together with the corresponding predictions of the fitting model in the case it was in perfect agreement with CFD. In addition, the lines corresponding to the maximum ±10% deviation between the fitting model predictions and the corresponding CFD results (black dashed lines) are also indicated.

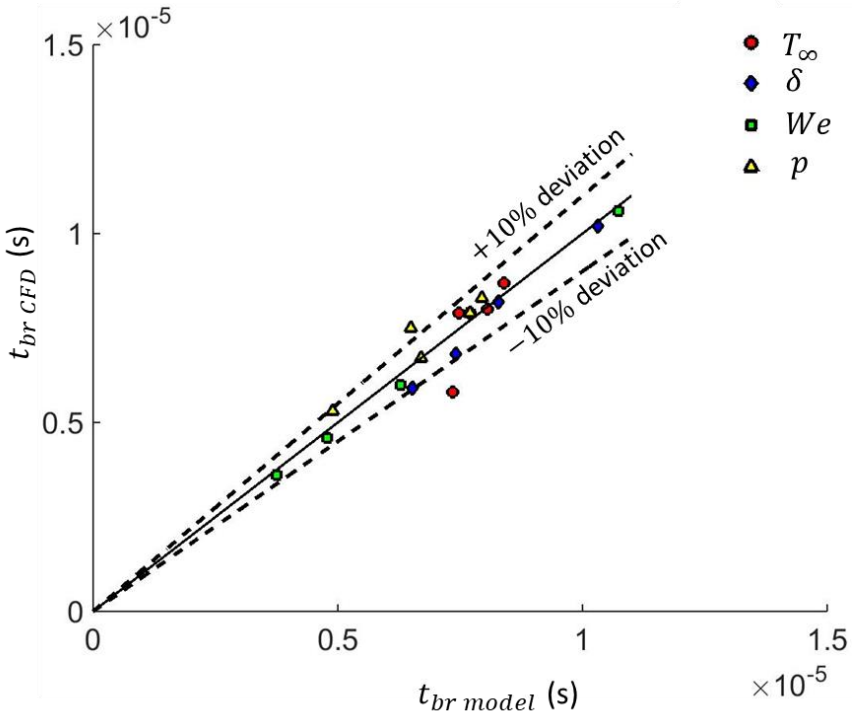

Figure 2. Emulsion breakup time as predicted by Eq. 1 (black solid line) alongside with ±10% deviation lines (black dashed lines) and the CFD simulations (scatter symbols)

3.2 Parametric study with We and $p - T$ conditions

The aerodynamic-induced breakup of a neat fuel droplet is typically characterized by the Weber (We) and Ohnesorge (Oh) numbers; the Reynolds number and the fuel-to-gas density (ε) and viscosity (N) ratios [46]. The shear breakup timescale $t_{sh} = D\sqrt{\varepsilon}/u_g$ is indicative of the time needed for breakup to be

completed [47], while the breakup initiation time can be predicted by the relationship proposed in [48] (among others):

$$t_{aero} = t_{sh} \cdot 8.95 \cdot We^{-0.352} Re^{-0.086} \left(\frac{1}{1 + \left(\rho_f / \rho_g\right)^{-0.5}} \right) \cdot \left(1 + 2.36 \cdot Oh^{0.93}\right) \quad (4)$$

This relationship is employed in order to compute the aerodynamic-induced breakup time of a neat HFO droplet and compare it with the emulsion-induced breakup time (Eq. 1), for the range of We numbers tested. The left panel of Figure 3 shows that t_{aero} (black dashed line) decreases strongly with increasing We, which is in accordance with several past studies [48, 49], while a weak decreasing dependence of the emulsion breakup on We is observed (black solid line). The difference between t_{br} and t_{aero} decreases as We increases; however it is important to mention that emulsion breakup occurs 3-5 times faster than the aerodynamic breakup for the conditions examined. This difference is in agreement with the results of [32]. The relative duration of heating (t_h; red dashed line) and growth (t_{grow}; blue dash-dot line) times, for the range of We numbers examined, is also shown in Figure 3. The heating time decreases exponentially as We increases due to the increase of convection, while bubble growth time slightly changes. Moreover, it is observed that for low We numbers ($We < 50$), the total emulsion breakup time (black solid line) depends more on t_h compared to t_{grow}, while the latter becomes more significant as the We increases. However, the relative duration of the aforementioned times is a strong function of the emulsion configuration considered. In emulsion droplet realised in fuel sprays, the embedded water droplets could be smaller and located closer to the HFO-gas interface (see following subsection). In such a configuration, the duration of the aforementioned times may be quite different. In the right pane of Figure 3, the aforementioned time predictions are presented again (t^*) but non-dimensionalised with the shear timescale t_{sh}. The latter varies with gas stream velocity u and thus with We, so different curves are illustrated compared to that in the left panel.

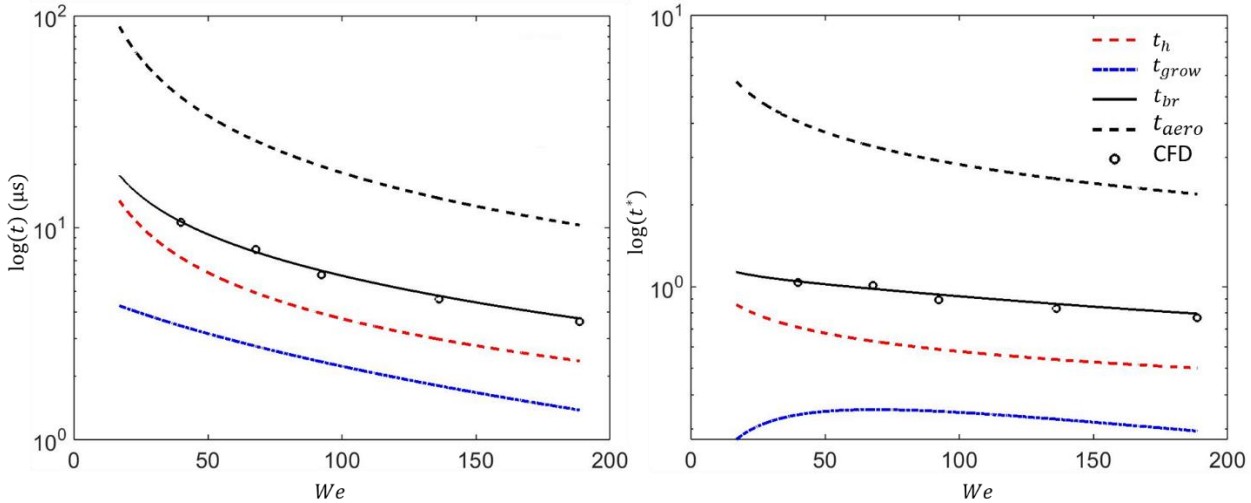

Figure 3.Dimensional (left panel) and non-dimensional (right panel) breakup time (black solid line) of an emulsion droplet alongside with heating (red dashed line) and bubble growth (blue dash-dot line) times predicted by the semi-empirical model and CFD simulations (black scatter symbols) against We. Black dashed line indicates breakup initiation time of a neat HFO droplet

Next, the fitting model is used to investigate the effect of ambient conditions on emulsion breakup time. The latter is computed for a wide range of temperature and pressure values encountered in marine diesel engines. Figure 4a shows on the $p-T$ diagram the breakup time; We and δ are constant and equal to that of ref case (Table 1). It is clear that the breakup time decreases as T_∞ increases while there is no clear pattern with pressure. The heating time, shown on Figure 4b, is shorter with increasing temperature (T_∞) and longer with increasing pressure. When the latter decreases, the embedded water droplet can reach faster its saturation temperature (T_{sat}); this trend is expressed through the f_T coefficient in Eq. 2 (see Appendix A). Finally, the bubble growth time t_{grow}, shown in Figure 4c, slightly increases with temperature while it varies non-monotonically with pressure in the examined range of 30-50 bar. The latter trend occurs because the variation in pressure affects, is a function of the inverse trends expressed by the coefficient g_P (see Appendix B) and the growth constant β in Eq. 3. Overall, minimum values of emulsion breakup time are predicted for maximum $p-T$ values, while its magnitude is determined mainly by the heating time period (Figure 4c) which is an order of magnitude higher ($\backsim 10^{-6}$ s) compared to the bubble growth time ($\backsim 10^{-7}$ s).

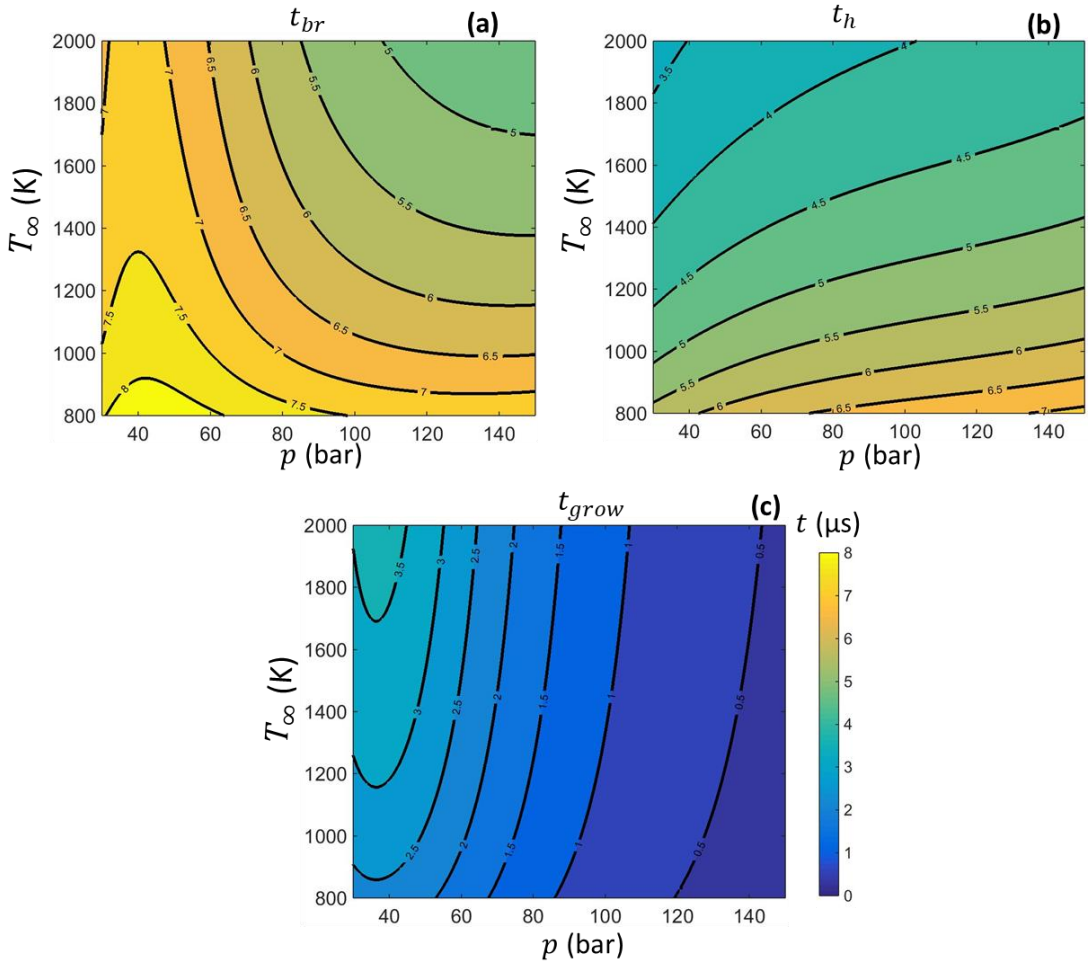

Figure 4. Predicted heating (a), bubble growth (b) and breakup (c) times breakup times on p-T diagram; ($We = 68, \delta = 0.06, D_w/D_f = 0.2$)

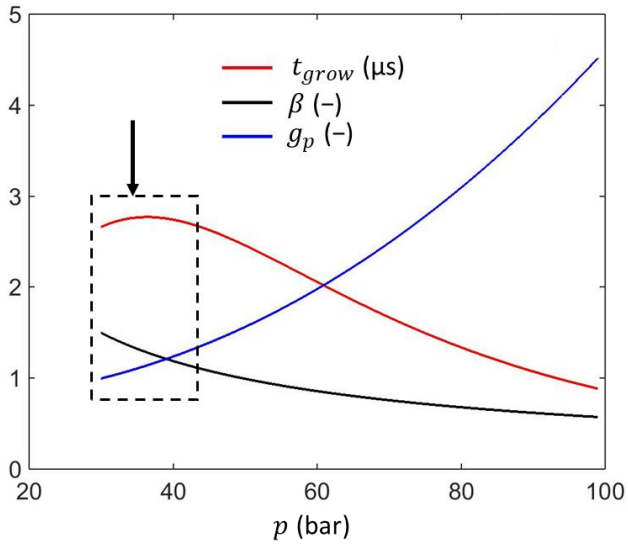

Figure 5. Dependence of t_{grow} (red line), β (black line) and g_p (blue line) on pressure ($T_\infty = 1000$ K).

3.3 Extrapolation to emulsion configurations not studied with CFD

In actual emulsion droplet configurations, several water micro-droplets will be dispersed inside the host fuel droplet. Some of them will be quite close to the fuel-gas interface and thus, will be the first to be subjected to water-vapor formation and growth. The minimum surface depth value investigated here with CFD simulations is $0.02R_f$, while the size of the embedded droplet used is $0.2R_f$, corresponding to 0.5μm and 5μm, respectively. However, these length scales can be at least an order of magnitude smaller in reality.

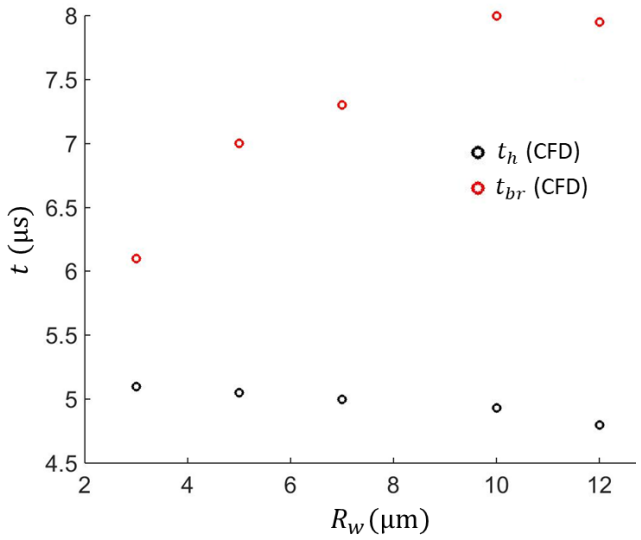

Figure 6. Heating (black scatter symbol) and breakup (red scatter symbol) time of an emulsion droplet against the radius of the water droplet.

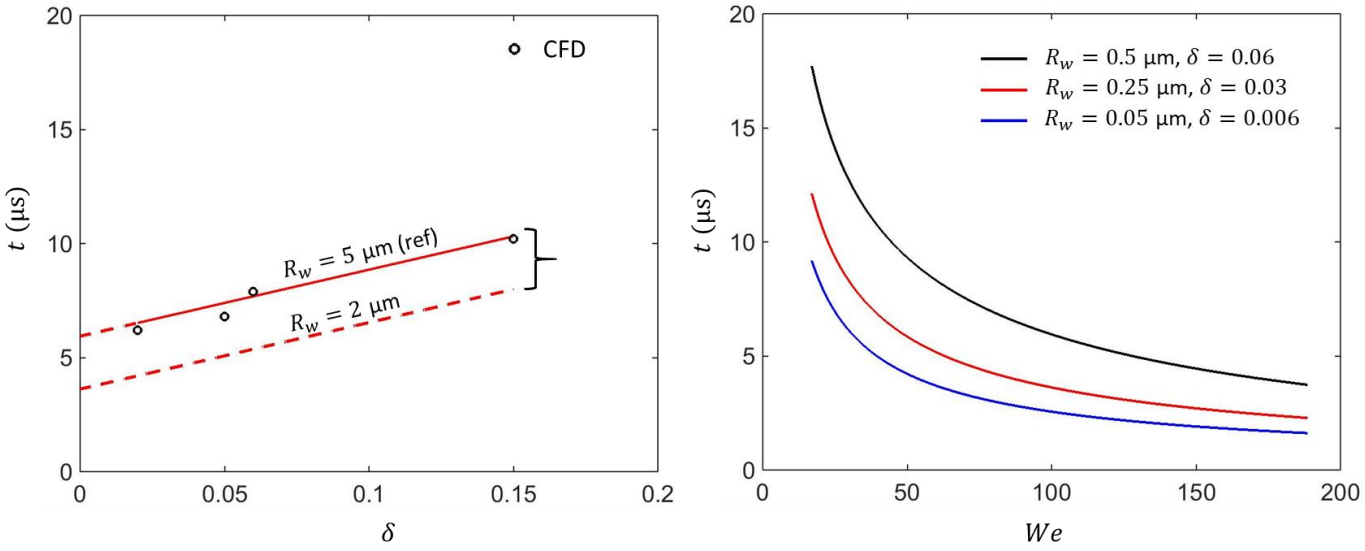

Figure 7. Left panel: Emulsion breakup initiation time against water droplet surface depth for two different water droplet sizes at $We = 68$. Right panel: Emulsion breakup initiation time against We for three sets of water droplet surface depth and size.

Numerical simulations obtained for the minimum surface depth and various water sub-droplet sizes (Figure 6) indicate that the heating time (t_h) remains unaffected (which can be expected), while the bubble growth time (t_{grow}) seems to follow the R_w^2 law indicated by Eq. 3. In the left panel of Figure 7, the solid lines refer to the CFD model range, while the dashed ones refer to those extrapolated with the fitting model (for δ values up to 0.15). Overall, it is observed that the breakup time increases with δ in a linear way, at least for the sizes examined; this is expected since as δ increases, the heat flux has to travel a larger distance and thus, the breakup process is decelerated. This pattern is in agreement with recent CFD and analytical model results [25, 26, 30]. Moreover, it seems that for smaller water droplet sizes, the breakup time slightly decreases, while its gradient with δ remains constant. In the right panel of Figure 7, emulsion breakup time is predicted against We for three different sets of water droplet sizes and surface depths. The difference in predicted t_{br} between the examined configurations diminishes as We increases.

3.4 Model performance for multiple parameter variation

As already mentioned, for the development of the current fitting model and the estimation of the coefficients incorporated in Eq. 2 and Eq. 3, only one parameter was changing at a time. In an effort to identify differences that may arise from the simultaneous change of more than one variable, four additional CFD simulations have been performed. The varying parameters are summarized in the following Table 2; the rest are kept the same to that of the reference case (Table 1).

	T_∞	p	We	d_h/R_f
Case 1	800	10	50	0.06
Case 2	800	10	215	0.06
Case 3	1500	140	215	0.06
Case 4	1500	140	50	0.06

Table 2. Operating conditions for the examined cases

The results obtained for these four cases for the breakup time are shown in Figure 8 together with the corresponding predictions from the fitting model; the ±10% deviation lines are also indicated. Model predictions seem to be in acceptable agreement with the CFD results, suggesting that the predictions of the fitting model can be trusted over the examined range of conditions even for simultaneous variation of the influential parameters considered.

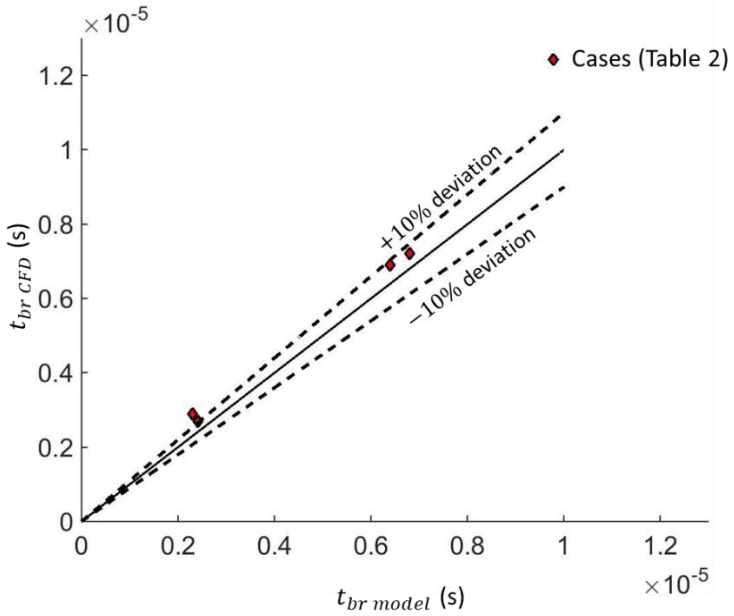

Figure 8. Emulsion breakup time as predicted by Eq. 1 (black solid line) alongside with ±10% deviation lines (black dashed lines) and the CFD simulations (scatter symbols)

4. Conclusions

A fitting model predicting the breakup initiation time of W/HFO droplets for $p-T$ conditions realized in marine Diesel engines and subjected to a gas flow stream has been presented; it's influence has been considered through the variation of the Weber number. The breakup initiation time has been expressed as the sum of two distinct time periods: (i) the time needed for the water sub-droplet to raise its temperature from T_0 to T'_{sat} and thus, for water vapor to form; this is mainly controlled by heat convection inside the parent fuel droplet; and (ii) the time period required for the formed water-vapor bubble to grow until the parent fuel droplet eventually breaks; this timescale is based on Scriven's analytical solution that predicts the growth of a water-vapor bubble inside an infinite water liquid pool. Calibration of the empirical coefficients of the derived model has been achieved via numerous CFD simulations obtained over the examined range of conditions. The obtained results have been found in acceptable agreement over the examined range of We numbers, $p-T$ conditions and surface depth of the water droplet inside the parent droplet. For low We numbers ($We<50$), results indicate that emulsion fuel breakup time occurs 5 times faster compared to aerodynamic breakup of a base fuel; this difference diminishes as We increases. In this We range, it is also observed that duration of heating time period is longer compared to that of vapor bubble growth. Emulsion breakup initiation time was found to increase linearly with the surface depth of the water droplet for the examined range of δ $(0-0.15)$. Regarding the effect of

ambient pressure and temperature on emulsion breakup time, it was observed that minimum values were obtained for high $p - T$ values.

Acknowledgement

Financial support from the MSCA-ITN-ETN of the European Union's H2020 programme, under REA grant agreement n. 675676 is acknowledged.

Appendix A. Derivation of heating time period (Eq.2)

The typical spray droplet velocity range (u_g) in HFO fueled engines is 10-100 m/s [50]; these conditions are characterized by $Pe >> 1$, implying that the heating of the fuel droplet is convection dominated. The timescale τ_{conv} provides a rough estimation of the time needed for the fuel droplet to heat up along a distance R_{oil} and raise its temperature from T_0 to T_∞. In the emulsion configuration examined (Figure 1; left panel), the embedded water droplet is located at surface depth (d_h) while it will start boiling when its surface temperature becomes equal to $T'_{sat} = T_{sat} + \Delta T_s$. Moreover, the droplet is expected to deform, since it is subjected to the action of aerodynamic forces. The effect of those variables on the heating time period has been examined with CFD simulations; the corresponding coefficients f_T, f_d and f_{We} are illustrated in Figure 9. It has also to be noted that the droplet heating time is also a function of the fuel thermal properties. Nevertheless, their effect is not included in the present study, since only one fuel was studied. Finally, the constant coefficients appearing in Eq. 2 were determined after fitting with CFD model results; the coefficient 3.6 is likely a function of Biot number, while the coefficient 8.9 appearing in f_δ is likely a function of fuel Peclet number.

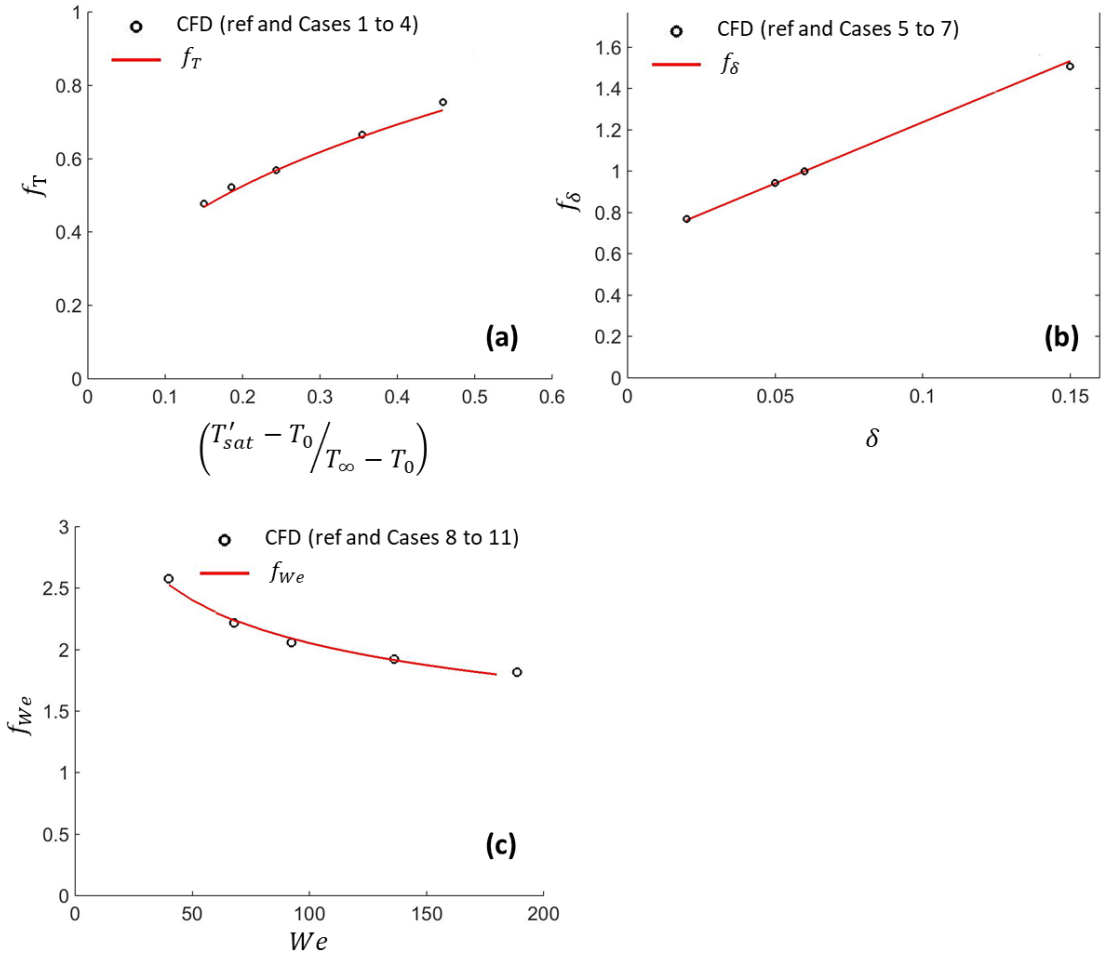

Figure 9. Nondimensional heating time predicted by CFD simulations (black scatter symbols) against $(T'_{sat} - T_0)/(T_\infty - T_0)$ parameter (left upper panel), nondimensional surface depth δ (right upper panel) and nondimensional We (lower panel). Fitting functions to the CFD predictions are illustrated with the red solid lines.

Appendix B. Derivation of bubble growth time period (Eq. 3)

The derivation of the bubble growth time period t_{grow} (Eq. 3) starts from Scriven's analytical solution, which reads:

$$R_b(t) = \beta\sqrt{a_w \cdot t} \tag{5}$$

This equation refers to idealized conditions in which a static vapor bubble grows inside an infinite water liquid pool. In the CFD cases examined, the bubble grows inside the water droplet with a much faster rate (Figure 10), which was found to depend on We and $p - T$ conditions. Thus, the growth rate constant β is multiplied by a set of corresponding coefficients $g_{T,}g_{P,}g_{We}$ and β; these are shown in Figure 11 (b, c, d). Regarding the bubble size at the breakup instant $R_b(t_{grow})$, a careful examination of all the CFD cases presented in Table 1 has shown that breakup occurs when the bubble reaches approximately half of the size of the embedded water droplet and depends slightly on We. The corresponding bubble size can be

expressed as $g_{br}R_w$, where g_{br} is the dimensionless bubble size at the breakup instant; the variation of this coefficient is shown in Figure 11 (a). Combining the aforementioned comments with Eq. 5, the latter recasts:

$$g_{br}R_w = g_T \cdot g_P \cdot g_{We} \cdot \beta\sqrt{a_w \cdot t_{grow}} \tag{6}$$

After solving for t_{grow}, Eq. 3 is derived.

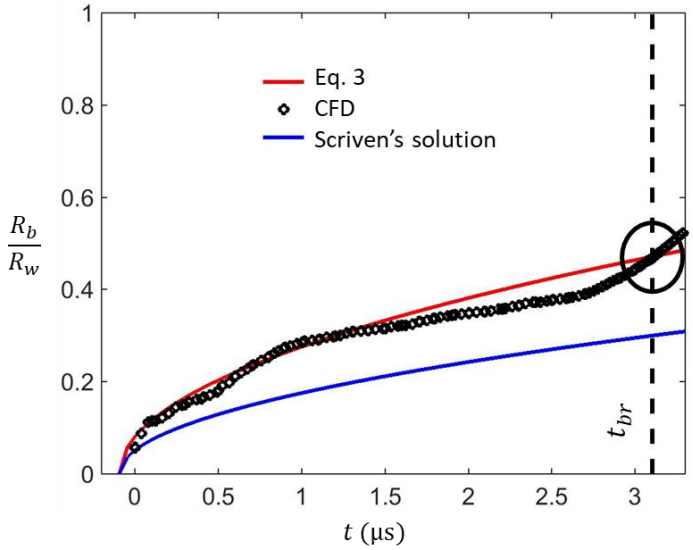

Figure 10. Nondimensional bubble radius as predicted by the CFD model (black scatter symbols), Scriven solution (blue solid line) and the current fitting model (red solid line)

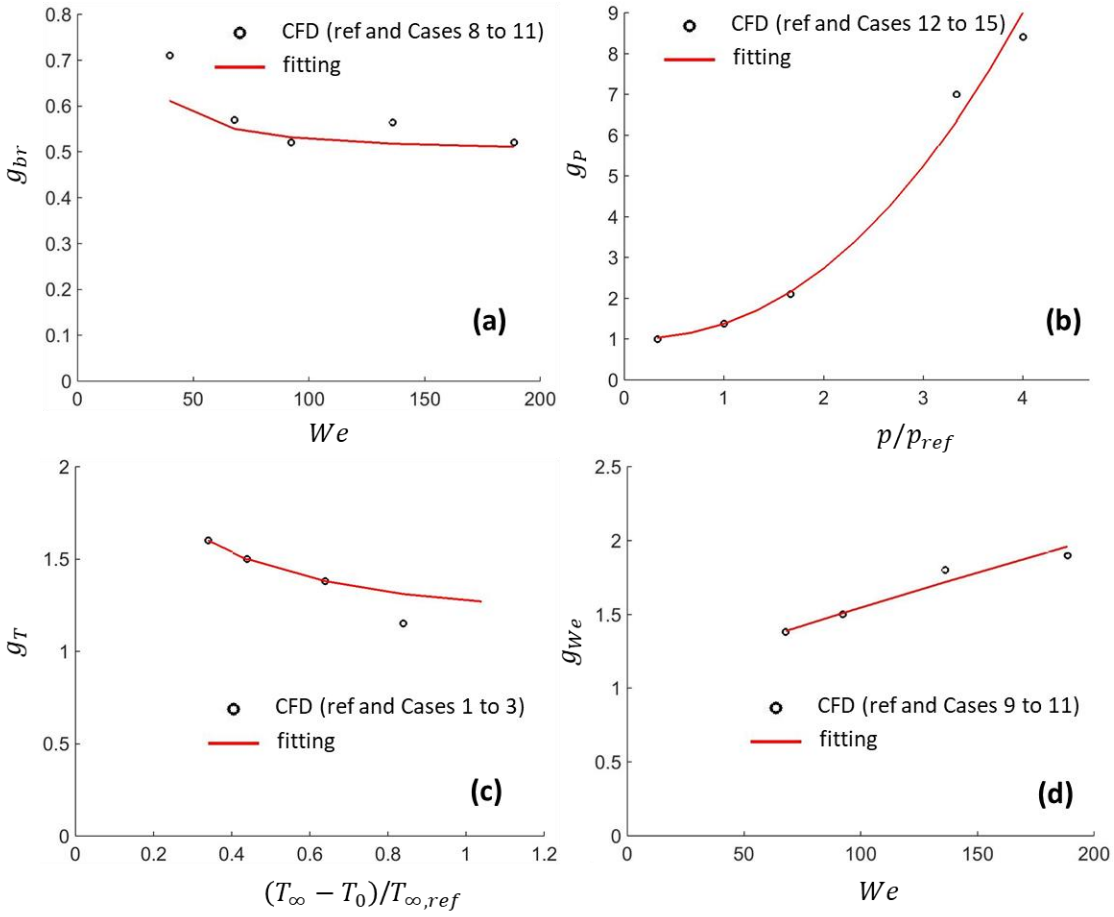

Figure 11. Correction factors g_{br} (left upper panel), g_p (right upper panel), g_T (left lower panel) and g_{We} (right lower panel) calibrated from the CFD model predictions (black scatter symbols)

References

1. Reitz, R., H. Ogawa, R. Payri, T. Fansler, S. Kokjohn, Y. Moriyoshi, A. Agarwal, D. Arcoumanis, D. Assanis, and C. Bae, *IJER editorial: The future of the internal combustion engine*. 2020, SAGE Publications Sage UK: London, England.
2. Zhou, X., E. Liu, D. Sun, and W. Su, *Study on transient emission spikes reduction of a heavy-duty diesel engine equipped with a variable intake valve closing timing mechanism and a two-stage turbocharger.* International Journal of Engine Research, 2019. **20**: p. 277-291.
3. Singh, R., T. Han, M. Fatouraie, A. Mansfield, M. Wooldridge, and A. Boehman, *Influence of fuel injection strategies on efficiency and particulate emissions of gasoline and ethanol blends in a turbocharged multi-cylinder direct injection engine.* International Journal of Engine Research, 2019: p. 1468087419838393.
4. Karim, Z.A.A., M.Y. Khan, A.R.A. Aziz, and F.Y. Hagos, *Attaining simultaneous reduction in NOx and smoke by using water-in-biodiesel emulsion fuels for diesel engine.* Platform: A Journal of Engineering, 2019: p. 1-21.
5. Avedisian, C. and R. Andres, *Bubble nucleation in superheated liquid—liquid emulsions.* Journal of colloid and interface science, 1978. **64**: p. 438-453.
6. Dryer, F. *Water addition to practical combustion systems—concepts and applications*. in *Symposium (international) on combustion*. 1977. Elsevier.
7. Lasheas, J., L. Yap, and F. Dryer. *Effect of the ambient pressure on the explosive burning of emulsified and multicomponent fuel droplets*. in *Symposium (International) on Combustion*. 1985. Elsevier.

8. Law, C., C. Lee, and N. Srinivasan, *Combustion characteristics of water-in-oil emulsion droplets.* Combustion and flame, 1980. **37**: p. 125-143.
9. Tsao, K. and C. Wang, *Puffing and micro-explosion phenomena of water emulsion fuels.* SAE transactions, 1986: p. 308-320.
10. Ivanov, V. and P. Nefedov, *Experimental investigation of the combustion process of natural and emulsified liquid fuels.* NASA Report 65N14944, 1962.
11. Ochoterena, R., A. Lif, M. Nydén, S. Andersson, and I. Denbratt, *Optical studies of spray development and combustion of water-in-diesel emulsion and microemulsion fuels.* Fuel, 2010. **89**: p. 122-132.
12. Park, S., S. Woo, H. Kim, and K. Lee, *The characteristic of spray using diesel water emulsified fuel in a diesel engine.* Applied energy, 2016. **176**: p. 209-220.
13. Zhu, M., Z. Zhang, Y. Zhang, P. Liu, and D. Zhang, *An experimental investigation into the ignition and combustion characteristics of single droplets of biochar water slurry fuels in air.* Applied energy, 2017. **185**: p. 2160-2167.
14. Shepherd, J.E. and B. Sturtevant, *Rapid evaporation at the superheat limit.* Journal of Fluid Mechanics, 2006. **121**: p. 379-402.
15. Shen, S., K. Sun, Z. Che, T. Wang, M. Jia, and J. Cai, *An experimental investigation of the heating behaviors of droplets of emulsified fuels at high temperature.* Applied Thermal Engineering, 2019. **161**: p. 114059.
16. Abdul Karim, Z., M.Y. Khan, and A.R.A. Aziz, *Evolution of Microexplosion Phenomenon in Parent–Child Droplets of Water in Biodiesel Emulsions Enhanced by Different Surfactant Dosages and Hydrophilic–Lipophilic Balance Values.* Journal of Energy Resources Technology, 2019. **141**.
17. Moussa, O., D. Francelino, D. Tarlet, P. Massoli, and J. Bellettre, *Insight of a water in oil emulsion dropl under Leidenfrost heating using laser-induced fluorescence optical diagnostics.* Atomization and Sprays, 2019. **29**.
18. Antonov, D., M. Piskunov, P. Strizhak, D. Tarlet, and J. Bellettre, *Dispersed phase structure and micro-explosion behavior under different schemes of water-fuel droplets heating.* Fuel, 2020. **259**: p. 116241.
19. Antonov, D.V., M.V. Piskunov, and P.A. Strizhak, *Explosive disintegration of two-component drops under intense conductive, convective, and radiant heating.* Applied Thermal Engineering, 2019. **152**: p. 409-419.
20. Antonov, D., M. Piskunov, and P. Strizhak, *Breakup and explosion of droplets of two immiscible fluids and emulsions.* International Journal of Thermal Sciences, 2019. **142**: p. 30-41.
21. Omar, M., T. Dominique, M. Patrizio, and B. Jérôme, *Investigation on the conditions leading to the micro-explosion of emulsified fuel droplet using two colors LIF method.* Experimental Thermal and Fluid Science, 2020: p. 110106.
22. Rao, D.C.K. and S. Basu, *Phenomenology of disruptive breakup mechanism of a levitated evaporating emulsion droplet.* Experimental Thermal and Fluid Science, 2020. **115**: p. 110086.
23. Fuchihata, M., T. Ida, and Y. Mizutani, *Observation of microexplosions in spray flames of light oil water emulsions. II. Influence of temporal and spatial resolution in high speed videography.* Nippon Kikai Gakkai Ronbunshu B Hen(Transactions of the Japan Society of Mechanical Engineers Part B)(Japan), 2003. **15**: p. 1503-1508.
24. Watanabe, H. and K. Okazaki, *Visualization of secondary atomization in emulsified-fuel spray flow by shadow imaging.* Proceedings of the Combustion Institute, 2013. **34**: p. 1651-1658.
25. Girin, O.G., *Dynamics of the emulsified fuel drop microexplosion.* Atomization and Sprays, 2017. **27**.
26. Sazhin, S., O. Rybdylova, C. Crua, M. Heikal, M. Ismael, Z. Nissar, and A.R.B. Aziz, *A simple model for puffing/micro-explosions in water-fuel emulsion droplets.* International Journal of Heat and Mass Transfer, 2019. **131**: p. 815-821.
27. Shusser, M. and D. Weihs, *Explosive boiling of a liquid droplet.* International journal of multiphase flow, 1999. **25**: p. 1561-1573.
28. Zeng, Y. and F.L. Chia-fon, *Modeling droplet breakup processes under micro-explosion conditions.* Proceedings of the Combustion Institute, 2007. **31**: p. 2185-2193.
29. Shepherd, J. and B. Sturtevant, *Rapid evaporation at the superheat limit.* Journal of Fluid Mechanics, 1982. **121**: p. 379-402.
30. Shinjo, J., J. Xia, L. Ganippa, and A. Megaritis, *Physics of puffing and microexplosion of emulsion fuel droplets.* Physics of Fluids (1994-present), 2014. **26**: p. 103302.

31. Shinjo, J., J. Xia, A. Megaritis, L. Ganippa, and R. Cracknell, *Modeling temperature distribution inside an emulsion fuel droplet under convective heating: a key to predicting microexplosion and puffing.* Atomization and Sprays, 2016. **26**.
32. Fostiropoulos, S., G. Strotos, N. Nikolopoulos, and M. Gavaises, *Numerical investigation of heavy fuel oil droplet breakup enhancement with water emulsions.* Fuel, 2020. **278**: p. 118381.
33. Stefanitsis, D., I. Malgarinos, G. Strotos, N. Nikolopoulos, E. Kakaras, and M. Gavaises, *Numerical investigation of the aerodynamic breakup of droplets in tandem.* International Journal of Multiphase Flow, 2019. **113**: p. 289-303.
34. Strotos, G., M. Gavaises, A.P. Theodorakakos, and G.C. Bergeles. *Evaporation of a suspended multicomponent droplet under convective conditions*. in *Proceedings of CHT-08 ICHMT International Symposium on Advances in Computational Heat Transfer*. 2008. Begel House Inc.
35. Strotos, G., I. Malgarinos, N. Nikolopoulos, and M. Gavaises, *Predicting the evaporation rate of stationary droplets with the VOF methodology for a wide range of ambient temperature conditions.* International Journal of Thermal Sciences, 2016. **109**: p. 253-262.
36. Strotos, G., I. Malgarinos, N. Nikolopoulos, and M. Gavaises, *Predicting droplet deformation and breakup for moderate Weber numbers.* International Journal of Multiphase Flow, 2016. **85**: p. 96-109.
37. Strotos, G., I. Malgarinos, N. Nikolopoulos, M. Gavaises, K.-S. Nikas, and K. Moustris, *Determination of the aerodynamic droplet breakup boundaries based on a total force approach.* International Journal of Heat and Fluid Flow, 2018. **69**: p. 164-173.
38. Ning, W., R.D. Reitz, R. Diwakar, and A.M. Lippert, *An Eulerian-Lagrangian spray and atomization model with improved turbulence modeling.* Atomization and Sprays, 2009. **19**.
39. Ubbink, O. and R. Issa, *A method for capturing sharp fluid interfaces on arbitrary meshes.* Journal of computational physics, 1999. **153**: p. 26-50.
40. Malgarinos, I., N. Nikolopoulos, and M. Gavaises, *Coupling a local adaptive grid refinement technique with an interface sharpening scheme for the simulation of two-phase flow and free-surface flows using VOF methodology.* Journal of Computational Physics, 2015. **300**: p. 732-753.
41. Kyriakides, N., C. Chryssakis, and L. Kaiktsis, *Influence of heavy fuel properties on spray atomization for marine diesel engine applications*. 2009, SAE Technical Paper.
42. Riazi, M., *Characterization and properties of petroleum fractions*. Vol. 50. 2005: ASTM international.
43. Hinze, J., *Fundamentals of the hydrodynamic mechanism of splitting in dispersion processes.* AIChE Journal, 1955. **1**: p. 289-295.
44. Hsiang, L.-P. and G.M. Faeth, *Near-limit drop deformation and secondary breakup.* International journal of multiphase flow, 1992. **18**: p. 635-652.
45. Scriven, L., *On the dynamics of phase growth.* Chemical engineering science, 1959. **10**: p. 1-13.
46. Guildenbecher, D., C. López-Rivera, and P. Sojka, *Secondary atomization.* Experiments in Fluids, 2009. **46**: p. 371.
47. Nicholls, J. and A. Ranger, *Aerodynamic shattering of liquid drops.* Aiaa Journal, 1969. **7**: p. 285-290.
48. Stefanitsis, D., I. Malgarinos, G. Strotos, N. Nikolopoulos, E. Kakaras, and M. Gavaises, *Numerical investigation of the aerodynamic breakup of Diesel and heavy fuel oil droplets.* International Journal of Heat and Fluid Flow, 2017. **68**: p. 203-215.
49. Pilch, M. and C. Erdman, *Use of breakup time data and velocity history data to predict the maximum size of stable fragments for acceleration-induced breakup of a liquid drop.* International journal of multiphase flow, 1987. **13**: p. 741-757.
50. Wadhwa, A.R., V. Magi, and J. Abraham, *Transient deformation and drag of decelerating drops in axisymmetric flows.* Physics of Fluids, 2007. **19**: p. 113301.